STATE-OF-THE-ART OF LAND DEFORMATION MONITORING USING DIFFERENTIAL SAR INTERFEROMETRY

M. Crosetto [a], B. Crippa [b], E. Biescas [a], O. Monserrat [a], M. Agudo [a]

[a] Institute of Geomatics, Av. del Canal Olímpic, s/n, Castelldefels, E-08860, Spain
(michele.crosetto, erlinda.biescas, oriol.monserrat, marta.agudo)@ideg.es
[b] Department of Earth Sciences, University of Milan, Via Cicognara 7, 20129 Milan, Italy - bruno.crippa@unimi.it

KEY WORDS: Remote Sensing, Satellite, Detection, Modelling, Software.

ABSTRACT:

In the last fifteen years the differential interferometric SAR, Synthetic Aperture Radar, (DInSAR) techniques have demonstrated their potential as land deformation measurement tools. In the last few years their capability has been considerably improved by using large stacks of SAR images acquired over the same area, instead of the classical two images used in the standard configurations. With these advances the DInSAR techniques are becoming more and more quantitative geodetic tools for deformation monitoring, rather than simple qualitative tools. The goal of the paper is to review the state-of-the-art of the spaceborne DInSAR-based land deformation monitoring. The airborne DInSAR is not considered in this work. The paper begins with a concise description of some basic DInSAR concepts, followed by a brief discussion of some important DInSAR applications. Then the state-of-the-art of DInSAR is analysed, by discussing few important technical issues, by addressing the issues of data and software availability, and by describing some relevant DInSAR results.

1. INTRODUCTION

This paper focuses on the land deformation measurement based on the differential interferometric Synthetic Aperture Radar techniques (DInSAR). Its goal is to review the state-of-the-art of the DInSAR techniques that make use of data acquired by spaceborne SAR sensors. The airborne DInSAR, which still plays a minor role in deformation applications, is not considered in this work.

The DInSAR techniques exploit the information contained in the radar phase of at least two complex SAR images acquired in different epochs over the same area, and that form an interferometric pair. Unlike a simple amplitude SAR image, which only contains the amplitude of the SAR signal, a complex SAR image contains two components per pixel, from which the amplitude and phase signal can be derived. The phase is the key observable of all interferometric SAR techniques. The repeated acquisition of images over a given area is usually performed by using the same sensor, e.g. the Envisat ASAR, or sensors with identical system characteristics, as it is the case of ERS-1 and ERS-2. Only in particular cases it is possible to make cross-interferometry by using images acquired with different systems. One example, which is discussed later in this paper, is given by ERS and Envisat ASAR, e.g. see Arnaud et al. (2003). Besides the compatibility of the systems used for the repeat pass DInSAR, the condition of forming interferometric pairs imposes a severe constraint on the acquisition geometry. In order to obtain coherent SAR image pairs, i.e. couples of SAR images whose interferometric phase is useful for digital elevation model (DEM) generation (using interferometric SAR, InSAR, techniques) or deformation monitoring, the images have to share almost the same image geometry. In fact, the simple fact that two images are not acquired exactly from the same point in space engenders a loss of coherence, which is called geometric decorrelation (Gatelli et al., 1994). For each SAR system there is a critical perpendicular baseline (the component of the vector that connects the two satellite positions during image acquisition, measured in the direction perpendicular to the SAR line-of-sight) which corresponds to a complete decorrelation of the interferometric phase. For instance, for ERS the critical baseline is about 1100 m: the employed baseline lengths are usually shorter, say of some hundreds of metres. An exception, as discussed in section 4, occurs using the so-called Persistent or Permanent Scatterers techniques that can exploit image pairs with baselines in the interval ± 1200 m (Colesanti et al., 2003a). Anyways, the constraint on the baseline plays a key role for all DInSAR applications.

In the following, the principle of the DInSAR technique is briefly summarized. A scheme of the image acquisition is shown in Figure 1, considering a single pixel footprint P:

- The sensors acquire a first SAR image at the time t_0, measuring the phase Φ_M. The first satellite and the corresponding image are usually referred as the master, *M*.
- Assuming that a land deformation D(t) occurs, which has a given evolution in time, the point *P* moves to P^1.
- The sensors acquire a second SAR image at the time t, measuring the phase Φ_S. The second satellite is usually referred as the slave, *S*.

The InSAR techniques exploit the phase difference of Φ_S and Φ_M, named interferometric phase $\Delta\Phi_{Int}$. Assuming that D(t) is naught, i.e. the terrain is stable and P' coincides with P, this phase is related to the distance difference $SP - MP$, which is the key element for the InSAR DEM generation. When the point moves from P to P^1 between two image acquisitions, besides the topographic phase component Φ_{Topo}, $\Delta\Phi_{Int}$ includes the terrain movement contribution, Φ_{Mov}. In the general case $\Delta\Phi_{Int}$ includes:

$$\Delta\Phi_{Int} = \Phi_S - \Phi_M = \frac{SP - MP}{\frac{\lambda}{4 \cdot \pi}} + \frac{SP^1 - SP}{\frac{\lambda}{4 \cdot \pi}} + \Phi_{Atm} + \Phi_{Noise} =$$

$$= \Phi_{Topo} + \Phi_{Mov} + \Phi_{Atm} + \Phi_{Noise},$$

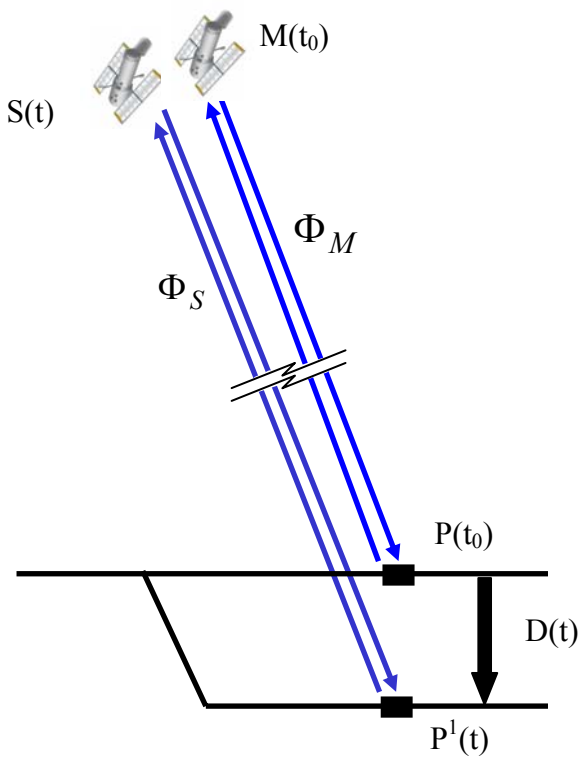

Figure 1: Principle of DInSAR for deformation measurement.

where Φ_{Atm} is the atmospheric contribution; Φ_{Noise} is the phase noise; SP^1 is the slave-to-P^1 distance; and λ is the radar wavelength. As mentioned above, using the topographic component Φ_{Topo} is possible to generate a DEM of the observed scene. In the DInSAR techniques the inverse transformation is used: if a DEM of the imaged scene is available, Φ_{Topo} can be simulated and subtracted from $\Delta\Phi_{Int}$, obtaining the so-called DInSAR phase $\Delta\Phi_{D-Int}$:

$$\Delta\Phi_{D-Int} = \Delta\Phi_{Int} - \Phi_{Topo\_Sim} = \\ = \Phi_{Mov} + \Phi_{Atm} + \Phi_{Res\_Topo} + \Phi_{Noise} \quad (1)$$

where Φ_{Topo_Sim} is the simulated topographic component, and Φ_{Res_Topo} represents the residual component due to errors in the simulation of Φ_{Topo}, e.g. errors in the employed DEM. In order to derive information on the terrain movement, Φ_{Mov} has to be separated from the other phase components. The techniques that use an external DEM in order to derive the topographic phase component use the so-called two-pass DInSAR configuration. There is another configuration, the three-pass interferometry, which can work without an a priori known DEM, but which requires at least three images acquired over the same scene (Zebker et al., 1994).

For a general review of SAR interferometry, see Rosen et al. (2000). This paper reviews different types of interferometric SAR techniques, for both DEM generation and land deformation measurement, analyses their theoretical aspects and limitations, and discusses their main applications. Another interesting review is given by Bamler and Hartl (1998), which focus on the signal theoretical aspects of InSAR, giving emphasis to the used mathematical models, to the statistical properties of the InSAR phase, and to the important topic of quality assessment.

In the following section are discussed some of the most important DInSAR applications. In the remaining part of the paper the state-of-the-art is analysed, by discussing the following topics:

- the number of SAR images used in the DInSAR procedures, which represents the main difference between the standard DInSAR techniques and the most advanced ones.
- the criteria used to select the pixels suitable to estimate the land deformation,
- the availability of DInSAR software tools,
- the satellite data sources for DInSAR applications,
- the key issue of quality and validation of the DInSAR results.

2. DInSAR APPLICATIONS

Since the first description of the technique, which was based on L-band SEASAT SAR data (Gabriel et al., 1989), the great potential of DInSAR for land deformation applications has been recognized. Of major interest were, in particular, some typical features of the remote sensing systems, like the wide areas covered by each image, the global coverage and the repeat observation capabilities, associated with the intrinsic high metric quality of the DInSAR observations. In fact, since the beginning, it was clear that the spaceborne DInSAR are able to measure small deformations with a high sensitivity, comparable to a small fraction of the radar wavelengths, which are in the order of centimetres to few tens of centimetres. Later on, other important characteristics were recognized. Firstly, the high spatial resolution capability of the SAR systems, which in particular cases allows the deformation monitoring of small features, like buildings or infrastructures, to be performed. Secondly, in the last years another relevant property has gained importance: the availability of large historical SAR datasets, which in the case of the ERS1/2 dataset covers almost 14 years.

In the last fifteen years many deformation-related DInSAR applications have been developed, and the capability of the D-InSAR techniques has been extensively documented. Hundreds of high level journal papers devoted to DInSAR have been published. A great contribution to this success certainly comes from the spectacular results achieved in different fields of geosciences. To the authors' knowledge, DInSAR-derived results have been published in tens of papers of Nature and Science, and have been featured several times in the covers of these prestigious scientific journals. Some of the most relevant DInSAR application fields are listed below:

- Seismology probably represents the field where the major number of scientific achievements have been obtained, including different types of coseismic studies, see e.g. (Massonnet et al., 1993; Peltzer and Rosen, 1995; Peltzer et al., 1999; Reilinger et al., 2000; Pedersen et al., 2001); postseismic deformation studies (Peltzer et al., 1996; Massonnet et al., 1996; Jónsson et al., 2003), and the monitoring of aseismic (Rosen et al., 1998) and interseismic tectonic events (Chorowicz et al., 1995; Wright et al., 2001; Colesanti et al., 2003a). It is worth emphasising that some of the above applications are characterized by very small deformations, e.g. less than 1 mm/yr for some aseismic and interseismic events. As it is described later in this paper, such types of deformations can only be achieved by using advanced DInSAR processing and analysis tools.
- Vulcanology represents another relevant application field, with several studies of volcanic deflation and uplift, e.g. see (Massonnet et al., 1995; Amelung et al., 2000; Lu et al., 2000; Salvi et al., 2004). Several examples of DInSAR

applications to volcanology are described in Massonnet and Sigmundsson (2000).

- Glaciology. Different researches have been conducted in this domain, mainly on the ice sheets of Greenland and Antarctica. They included InSAR ice topography measurements (Kwok and Fahnestock, 1996; Joughin et al., 1996); ice velocity measurements (Goldstein et al., 1993; Joughin et al., 1995; Joughin et al., 1998; Mohr et al., 1998); and other glaciological applications, like the determination of the discharge of glaciers (Rignot et al., 1997; Joughin et al., 1999).
- Landslides. In this important application less results have been achieved, mainly due to the loss of coherence that usually characterises the landslides areas. However, with the Persistent Scatterers techniques for some types of landslide phenomena it seems to be possible to perform DInSAR deformation measurements. The most relevant results are described in Carnec et al. (1996); Fruneau et al. (1996); Colesanti et al. (2003b), Hilley et al. (2004), and Delacourt et al. (2004).
- Ground subsidences and uplifts due to fluid pumping, construction works, geothermal activity, etc. have been described in several papers, see e.g. Massonnet et al. (1997); Galloway et al. (1998); Jonsson et al. (1998); Amelung et al. (1999); Wicks et al. (2001); Hoffmann et al. (2001); Crosetto et al. (2003); Lanari et al. (2004). Most of the published results concern urban areas, over which DInSAR data remains coherent even with large observation periods. With the advent of the Persistent Scatterers techniques it is expected to get more and more deformation monitoring results outside the urban, suburban and industrial areas.

Finally, comprehensive reviews of different DInSAR geophysical applications are provided by Massonnet and Feigl (1998) and Hanssen (2001). An interesting link, where the latest DInSAR results based on data acquired by the ERS and Envisat satellites is given by eopi.esa.int/esa/esa.

3. DInSAR and ADVANCED DInSAR TECHNIQUES

A large part of the important DInSAR application results mentioned in the previous section have been achieved by using the standard DInSAR configuration, i.e. by analysing a single differential interferogram derived from a pair of SAR images. This is the simplest DInSAR configuration, which often is the only one that can be implemented, due to the limited data availability for several practical deformation measurement applications. However, as it is discussed later, the standard two-image configuration suffers important limitations. Even if for some types of application it may provide valuable results, e.g. for the estimation of large, say from decimetres to meters, deformation patterns, in general it is necessary to be aware of its limitations. A remarkable improvement in the quality of the DInSAR results is given by the new DInSAR methods that make use of large sets of SAR images acquired over the same deformation phenomenon. These techniques, hereafter called Advanced DInSAR (A-DInSAR) techniques, represent an outstanding advance with respect to the standard ones, both in terms of deformation modelling capabilities and quality of the deformation estimations:

- Temporal deformation modelling. As it is illustrated in Figure 2, a standard DInSAR technique, which samples temporally a given deformation phenomenon with only two samples, a master image M and a slave one S, is only able to estimate the integrated deformation:

$$D_I(\Delta T) = D(t_S) - D(t_M),$$

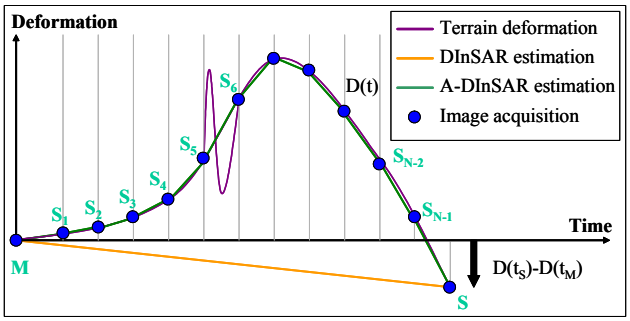

Figure 2. Temporal sampling of a deformation phenomenon performed with the DInSAR and A-DInSAR techniques.

or, equivalently, the linear deformation velocity between t_M and t_S. In contrast, the A-DInSAR techniques are in principle able of providing a whole description of the temporal behaviour of the deformation field at hand. This capability is clearly limited by the number N and the temporal distribution of the available SAR images. For instance, the highly non linear deformation that occurs between the acquisitions S_5 and S_6 in Figure 2 cannot be measured with the available SAR image acquisition.

- Quantitative vs. qualitative DInSAR. There is a second fundamental difference between DInSAR and A-DInSAR techniques. The standard configuration represents a zero-redundancy case, where it is not possible to check the presence of the different error sources that may affect the interferometric observations, or, equivalently, it is impossible to separate the movement component from the other phase components, see Formula (1). For this reason the estimations derived with this configuration have, in general, a quantitative character and have to be employed with care. Note that in different applications some external information on the deformation under analysis may be available (e.g. a priori knowledge of stable areas, of the shape of the deformation field, etc.), which can considerably help in interpreting the DInSAR results. In contrast, the A-DInSAR methods may implement suitable data modelling and analysis procedures that associated with appropriate statistical treatments of the available DInSAR observations make possible the estimation of different parameters. In addition to this extended capability, the A-DInSAR techniques take usually advantage of a high data redundancy, which allows quantitative DInSAR results to be achieved, both in terms of precision and reliability. The main parameters estimated by the DInSAR are briefly discussed below.

1) By proper modelling the phase component due to terrain movement Φ_{Mov}, it is possible to estimate the spatial and temporal evolution of the deformation. The modelling strategies are strictly dependent on the type of application at hand. Anyways, the ability to fully describe a deformation phenomenon depends temporally on number of available images, and spatially on the availability of "good pixels", i.e. pixels which are characterized by a low level of phase noise, Φ_{Noise}. This aspect is discussed in detail in the following section. Often the temporal evolution of the deformation is modelled with linear functions, e.g. see (Ferretti et al., 2000; Ferretti et al., 2001). Crosetto et al. (2005) model the deformation by stepwise linear functions, whose parameters are computed by least squares adjustment. Other approaches allow a more complex description of the temporal behaviour of the deformation, see e.g. (Berardino et al., 2002; Mora et al., 2003; Colesanti et al., 2003a; Lanari et al. 2004).

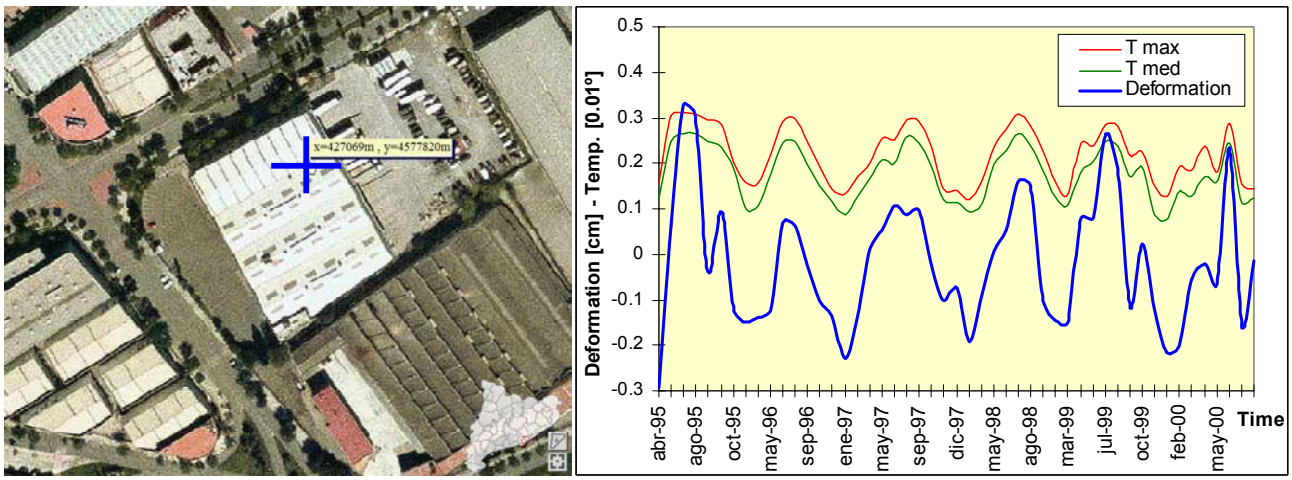

Figure 3: Example of estimation of the temporal evolution of deformation: deformation of the roof of an industrial building located in the metropolitan area of Barcelona. Input data: 49 ERS-1 and ERS-2 SAR that cover the period 1995 to 2001. The deformation is probably due to thermal dilation of the portion of the observed roof. Data courtesy of Altamira Information.

The complete estimation of the temporal evolution of deformation represents a remarkable improvement of the A-DInSAR techniques with respect to the standard DInSAR results. Figure 3 shows an example which concerns the roof of an industrial building located in the metropolitan area of Barcelona. This result was obtained in the frame of an ESA funded Project named "Development of algorithms for the exploitation of ERS-Envisat using the SAR permanent scatterers technique", coordinated by Altamira Information (www.altamira-information.com). It was obtained by Altamira, one of the few commercial companies worldwide that has A-DInSAR capabilities, and was validated at the Institute of Geomatics. In this case 49 ERS-1 and ERS-2 SAR images were used, which cover the period 1995 to 2001. One may appreciate the highly non-linear behaviour of deformation. There is a high correlation coefficient between the deformation pattern and the time series of mean and maximum temperature of Barcelona in the acquisition days of the 49 images. This indicates that the deformation is probably due to thermal dilation of the portion of the observed roof. It is worth noting the magnitude of the deformation oscillation, which range in the interval ± 3 mm: this result is useful to get an idea of the sensitivity of the A-DInSAR outcomes.

2) The residual topographic error e_{Topo} represents another interesting type of parameter that can be estimated by using the A-DInSAR techniques. The residual topographic error is given by the difference between the true height of the scattering phase centre of a given pixel, and the height given by the employed DEM or digital terrain model (DTM). The information on this parameter is contained in the residual phase component due to errors in the topographic phase simulation $\Phi_{\mathrm{Re}s\_Topo}$. This component depends linearly on the residual topographic error (Ferretti et al., 2000), and its magnitude on a given interferogram is modulated by its perpendicular baseline $B_{\perp}$. Therefore, given a set of interferograms, the wider is the spectrum of $B_{\perp}$, the better is the configuration to estimate e_{Topo}. This parameter plays an important role only for two specific goals: for A-DInSAR modelling purposes, and for geocoding purposes. As said above, $\Phi_{\mathrm{Re}s\_Topo}$ can be explicitly modelled, i.e. can be explained by estimating one parameter e_{Topo} per each pixel. If this parameter is disregarded, $\Phi_{\mathrm{Re}s\_Topo}$ will contribute to the non modelled part of $\Delta\Phi_{D-Int}$, i.e. it will go in the residuals, or will affect the estimation of other parameters of interest. Therefore, the estimation of e_{Topo} results in a net benefit for modelling. The second important use of e_{Topo} is the implementation of advanced geocoding procedures for the A-DInSAR products. The standard methods simply employ the same DEM or DTM used in the simulation of Φ_{Topo_Sim} to geocode the DInSAR products. That is, they use an (often rough) approximate value of the true height of the scattering phase centre of a given pixel, which results in a location error during the geocoding. By using the estimated residual topographic error this kind of error can be largely reduced, thus achieving a more precise geocoding. This may considerably help the interpretation and the exploitation of the A-DInSAR results. An example of A-DInSAR geocoding is shown in Figure 4. It concerns the area of the Stadium of Naples (Italy). The upper image shows the location of the DInSAR measured pixels obtained by employing a standard DEM-based geocoding, while the lower image shows the precise location, which was computed by using the residual topographic error, see for details Lanari et al., (2004).

The formal precision that can be achieved in the estimation of e_{Topo} is a function of the distribution of the $B_{\perp}$. Using large baselines, which range in the interval ± 1200 m, Colesanti et al. (2003a) achieve a standard deviation of the estimated e_{Topo} that is less than 1 m. Despite the importance of the above uses of e_{Topo}, it is important to note that this parameter describes a rather specific feature, i.e. the height of the radar scattering phase centre, which depends on several factors that drive the dominant mechanism of scattering, e.g. orientation, size, shape, density and dielectric constant. This means that e_{Topo} cannot in general be used to improve the quality of the DEM used in the A-DInSAR procedure. It can only be used to derive a kind of improved "radar DEM". Furthermore, it is worth noting that e_{Topo} is only estimated over the "good pixels" exploited by the A-DInSAR procedures.

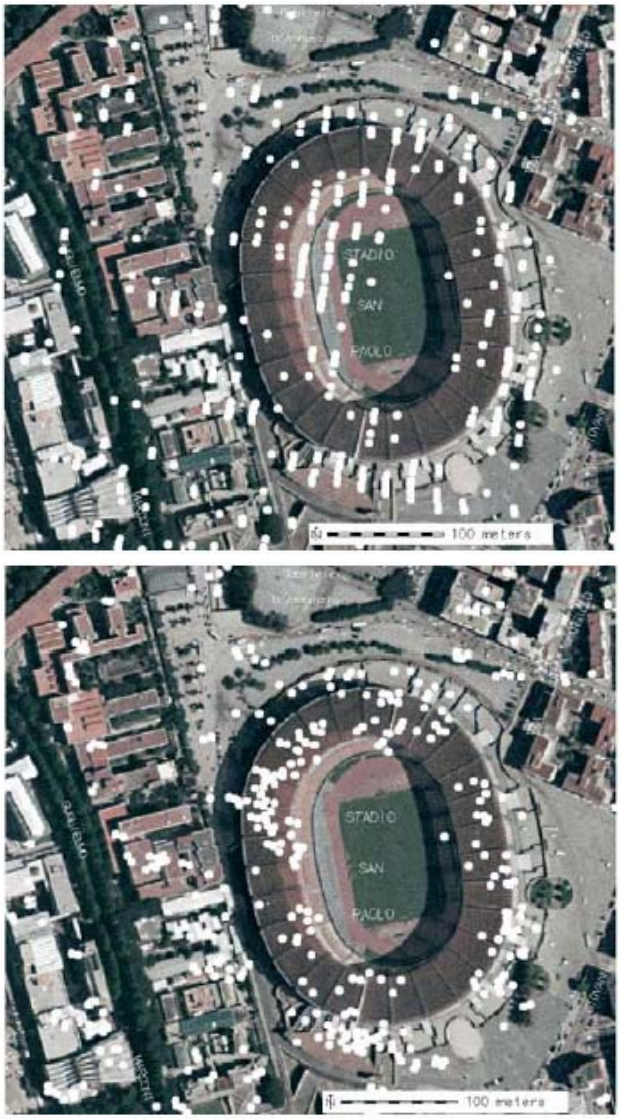

Figure 4: Example of advanced geocoding of A-DInSAR results over the area of the San Paolo Stadium of Naples (Italy). Pixel location without (above) and with (below) the correction based on the residual topographic error. An optical image of the area is on the background. This result was achieved by using an A-DInSAR technique described in Lanari et al., (2004) with 55 ERS images. (Images courtesy of Dr. Riccardo Lanari from IRECE-CNR, Naples, Italy).

3) The A-DInSAR techniques can estimate the atmospheric phase contribution of each image of the used SAR stack (this contribution is sometimes called Atmospheric Phase Screen, APS), starting from the phase component Φ_{Atm} of the interferograms derived by combining pair wise the SAR images. Even if this information is usually useless for other applications, it is fundamental to achieve an accurate DInSAR modelling and thus to properly estimate the deformation contribution. In fact, only if APS contributions are properly estimated and removed it is possible to avoid the strong degradation of the DInSAR quality caused by the atmospheric effects. The A-DInSAR strategies used to estimate the APS contributions usually exploit the spatio-temporal correlation characteristics of the APSs, i.e. that the atmospheric effects are usually uncorrelated in time, while they are spatially smooth, e.g. see Ferretti et al., (2000).

4. PIXEL SELECTION: COHERENCE vs. PERSISTENT SCATTERERS

Even if SAR sensors perform a regular 2D sampling of the terrain, only the pixels characterized by a low level of phase noise, Φ_{Noise}, are exploited to derive the deformation estimations. This requires adopting a pixel selection criterion. As mentioned above, the loss of coherence results in a noisy interferometric phase. During the interferometric process it is possible to estimate, for each interferogram, the coherence (i.e. the correlation) of the two images that form the given interferogram. The standard DInSAR techniques use this information for the pixel selection, i.e. they perform a coherence-based pixel selection. Note that the same criterion is used by other more advanced DInSAR techniques based on SAR image stacks, e.g. see Le Mouélic et al., (2005), and by some A-DInSAR techniques (Berardino et al., 2002; Mora et al., 2003; Lanari et al., 2004; Crosetto et al., 2005). Examples of advanced results achieved by one of these A-DInSAR techniques can be found in www.irea.cnr.it/webgis/terra.html. Another important class of A-DInSAR techniques use as a pixel selection criterion the stability of the SAR amplitude (Ferretti et al. 2000). The points selected with such a criterion are usually referred to as Permanent or Persistent Scatterers (PS). Note that the term Permanent Scatterers is directly associated with a patented technique. Therefore, the second term, Persistent Scatterers, is the more appropriate. Related to this, it is important to clarify two important points on the so-called Permanent Scatterers technique, which was developed and patented by the Politecnico di Milano (Italy), and which now is exclusively licensed to TRE (www.treuropa.com), a spin-off company of this technical university. Often is repeated the following question: do you use DInSAR or Permanent Scatterers? The answer is that the Permanent Scatterers is a DInSAR technique, and more precisely it is just one of the A-DInSAR techniques that work with large image stacks. The second point that often generate confusion is this that the term "Permanent Scatterers", which sometimes is used as synonymous of A-DInSAR, is associated with a specific pixel selection criterion. This may be misleading, because, as already mentioned above, there are different A-DInSAR techniques that use a coherence-based pixel selection criterion. The authors have developed a complete A-DInSAR chain, which works indifferently with both the coherence or amplitude based selection criteria.

The choice of the selection criterion depends on the application at hand. The coherence-based A-DInSAR methods work well over long-term coherent areas: urban, suburban and industrial areas. Their major limitation is that most spaceborne sensors are operated in C-band, see Table 2, a frequency in which decorrelation effects are strong in particular over vegetated areas. Furthermore, the repeat cycles of these satellites are rather long: this causes a loss in coherence, and usually prevents the generation of deformation results outside the urban areas. Figure 5 shows a result derived with a coherence-based A-DInSAR technique. The deformation velocity field is superposed to a SAR amplitude image of the same area. In this case a kind of low cost analysis has been performed, using 13 ERS SAR images, see for details Crosetto (2004). Other coherence-based DInSAR results are described in Biescas et al. (2005). In this case different unknown subsidence phenomena have been discovered: this example shows the potential of DInSAR as an "early detection tool" of deformations. Figure 6 shows a zoom of Figure 5 over an industrial area. In this second image there are geocoded deformation velocities, which are superposed to an orthoimage.

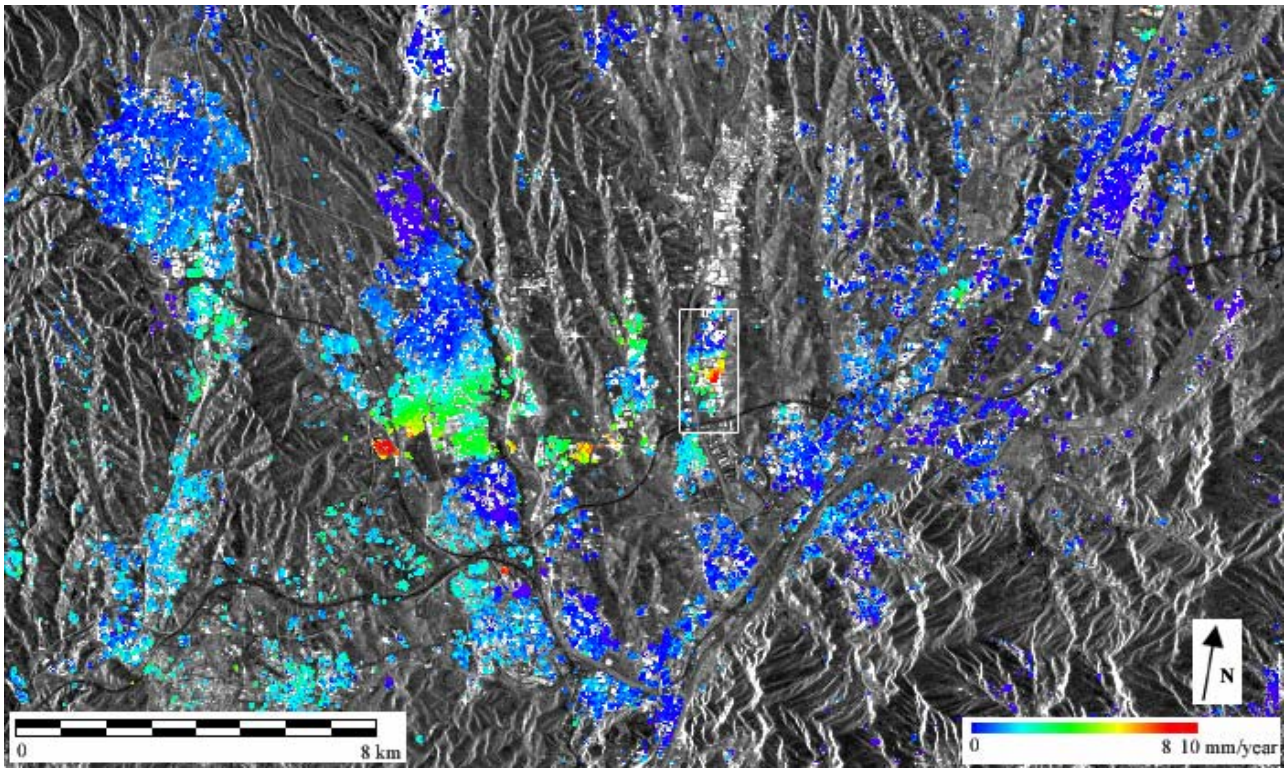

Figure 5: Coherence-based A-DInSAR analysis over an area of 28 by 12 km, based on 13 ERS images: vertical deformation velocity in the time period June 1995 and August 2000. The velocity, in colour, is superposed to a SAR amplitude image of the same area. The areas in grey values are those where no velocity estimation is possible due to coherence loss.

One may notice in Figures 5 and 6 that over a large part of the analyzed area the deformation cannot be measured, due to a lack of coherence. This result could be probably improved by using a PS-based technique, whose main advantage is to exploit all the coherent targets of the covered scene, included those located outside the coherent areas. The coherence of a given pixel is estimated over a window centred on the same pixel: if a single and very coherent target (e.g. a small man-mad object) is located in a very noisy area (e.g. a grass field) it will have an estimated low coherence value. This does not occur with the PS techniques, which work at full resolution and which select the pixels without considering the neighbourhood pixels. An example is illustrated in Figure 7, which concerns a very thin, say 12 m large, dike of the port of Barcelona. By using a PS-based approach it is possible to perform a deformation monitoring of such a structure. The same cannot be done by adopting a coherence-based technique.

5. AVAILABLE SOFTWARES

The importance that DInSAR is gaining as a deformation monitoring tool is reflected in the number of available softwares that have DInSAR analysis capabilities. Some of them are listed in Table 1. Note that this list is not exhaustive and, more importantly, that the reported information comes from publicly available documentation: this software has not been tested by the authors. The table does not include the software tools developed by the research centres specialized in A-DInSAR that are not commercialized or freely distributed for non-commercial purposes. Moreover, it is worth to underline that few specialized private companies hold very advanced A-DInSAR tools, which are not commercialized. This, for instance, is the case of TRE, based in Milan, and Altamira Information, located in Barcelona.

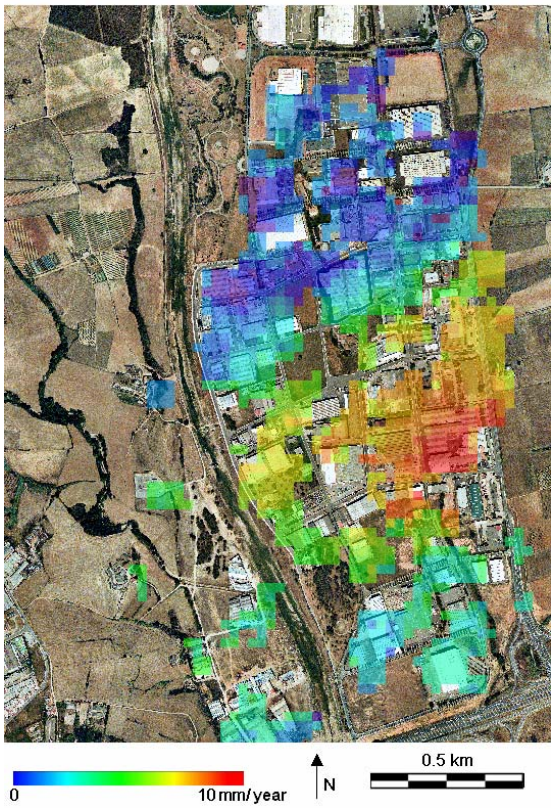

Figure 6: A-DInSAR analysis over an industrial area, whose location is shown by a white frame in Figure 5. The vertical deformation velocity field is superposed to a 1:5000 orthoimage of the Cartographic Institute of Catalonia.

The first two softwares listed in Table 1 are freely available for non-commercial purposes: DORIS, see a description in Kampes et al., (2003), and ROI_PAC. Both of them have their source code available. The DIAPASON is a command line software developed by a research group at the French CNES, which is suitable for advanced users. Some remote sensing software tools include specific modules for standard DInSAR analysis, i.e. the analysis based on single interferograms. This is the case of ENVI, while other packages e.g. ERDAS, seem to provide only tools for InSAR analysis. Example of A-DInSAR commercial tools are those sold by Vexcel and Gamma. This last company, which is based in Switzerland, besides selling its products, with included the possibility to buy the source code, provides A-DInSAR analysis services.

6. DATA AVAILABILITY

The availability of data acquired by spaceborne sensors represents a key issue for the successful use of the DInSAR technique and especially the A-DInSAR techniques that require large series of SAR images. Furthermore, for these techniques plays a fundamental role the image acquisition continuity over large time periods of the same sensor, or compatible sensors, e.g. ERS-1 and ERS-2. The continuity is needed in particular for all the applications characterized by small deformation rates, for those that require long-term deformation monitoring, and in general for the acceptation of the A-DInSAR techniques as operational land deformation monitoring tools. In Table 2 are reported the principal SAR missions and satellites that have demonstrated DInSAR capabilities. For each satellite are given at least two references to studies realized with its data and documented in the scientific literature. Besides the Seasat mission, which gave the data used to derive the first DInSAR results (Gabriel et al., 1989) but which however had a very short life, the satellite which has provided the data to fully demonstrate the DInSAR potentiality was ERS-1. This satellite has been operative for 10 years, and, more importantly, with its exact copy, ERS-2, has provided a valuable historical archive of interferometric SAR data, which has global spatial coverage and covers a time period of almost 14 years, with the first images that date back to summer 1991. Besides the four references given in the table, there are hundreds of high level scientific publications that demonstrate the success of the ERS mission.

The satellites that are currently operational are RADARSAT-1 and ENVISAT. Various space agencies are planning new missions for earth observation with microwave SAR sensors, e.g. RADARSAT-2 a mission of the Canadian Space Agency in cooperation with other partners; COSMO-SKYMED (Constellation of Small Satellites for Mediterranean basin observation) of the Italian Space Agency; and MAPSAR, a mission which is expected to have high spatial resolution L-band capabilities for polarimetry, and interferometry, see Schröder et al. (2005). A special mention is reserved by the continuity issue between the ERS and Envisat missions of the European Space Agency. It is in fact clear that it would be very useful to guarantee in the near future the continuity of the existing 14 year archive of interferometric SAR images. There is a temporal overlap between the ERS-2 and Envisat missions: this new instrument could in principle continue the success of the ERS satellites and increase the value of the archived ERS data. In reality, there is a big problem in mixing Envisat and ERS data: the two systems have slightly different radar frequencies, and this prevents the simple combination of their data (the interferometric phase is strongly dependent on the wavelength, and thus the radar frequency).

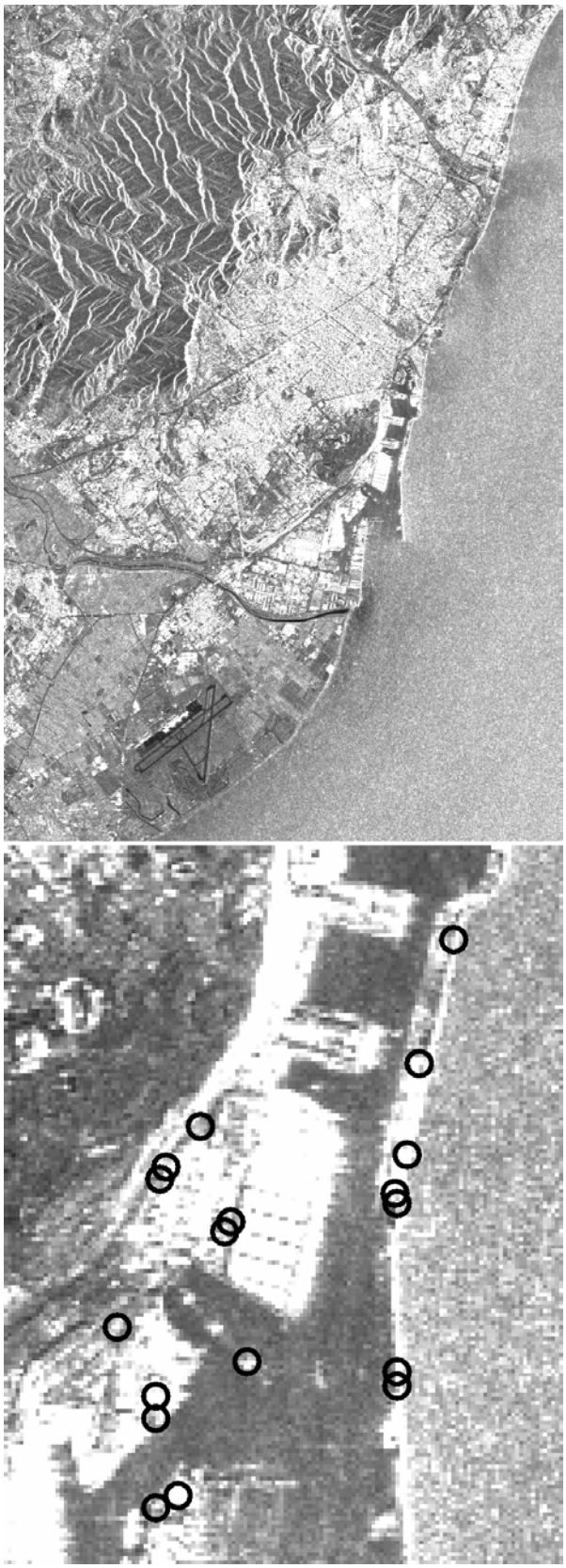

Figure 7: PS-based pixel selection over the Barcelona area. Amplitude SAR image of the city and zoom of the port, where several Persistent Scatterers are shown. Some of them lie on a very thin structure, the main dike of the port: over these PS it is possible to perform a deformation monitoring. Such structures cannot be measured by a coherence-based technique.

Software name	Company/ University	Web site/ type of licence	Platform and software characteristic	DInSAR capabilities
DORIS	TU Delft	enterprise.lr.tudelft.nl/doris free license for non-commercial purposes	Unix/Linux/WinXP (C++ source code available)	Standard DInSAR with ERS1/2, RADARSAT, ENVISAT, JERS data. Additional programs for unwrapping (Snaphu) and orbit processing (Getorb) are available
ROI_PAC	Berkley University	www.openchannelfoundation.org free license for non-commercial purposes	Unix/Linux (C and F90 source code available)	Standard DInSAR with ERS1/2, JERS
DIAPASON	Developed by CNES	www.altamira-information.com commercial licence distributed by Altamira Information	Linux/Win 95, 98, NT, 2000	Standard DInSAR with ERS1/2, JERS-1, RADARSAT, ENVISAT
ENVI	Research Systems Inc. (RSI)	www.rsinc.com/envi commercial licence	Unix/Linux/Win2000 and WinXP	Module of ENVI, SARscape, standard DInSAR with ERS1/2, JERS-1, RADARSAT, ENVISAT
VEXCEL 3DSAR	Vexcel Corporation	www.vexcel.com commercial licence	Unix/Linux/Windows	Module of the EV-InSAR, CTM - Coherent Target Monitoring, with advanced DInSAR capabilities with ERS1/2, JERS-1, RADARSAT, ENVISAT
GAMMA	Gamma	www.gamma-rs.ch/ commercial licence	UNIX, Linux, Windows Modular packages in ANSI-C language, code available	Advanced DInSAR with ERS1/2, JERS-1, SIR-C X-SAR, RADARSAT, ENVISAT

Table 1: Available softwares with standard DInSAR or advanced DInSAR capabilities.

In the last two years a big effort has been devoted to this topic, e.g. see Arnaud et al. (2003) which describe the generation of the first ERS-Envisat cross-interferogram. Without going into details, it is worth mentioning that combining ERS and Envisat data for A-DInSAR applications, i.e. using mixed image stacks of ERS and Envisat, under given conditions is possible, see some interesting results in Duro et al. (2005). In particular, this is possible by taking advantage of a special feature of the PS: that usually are much smaller than the resolution cell, and thus have a reduced geometric decorrelation due to the fact that the two SAR images are not acquired exactly from the same point.

7. DInSAR QUALITY and VALIDATION ISSUES

An important goal of the current A-DInSAR research is to provide deformation observations characterized by high quality standards (accuracy, precision and reliability), which are comparable with those of the observations coming from the geodetic techniques. As mentioned in previous sections, the above goal can only be achieved using a high observation redundancy (i.e. by using several SAR images of the same area), and by implementing appropriate data analysis tools. In the last few years there has been an increasing attention to the A-DInSAR estimation quality, e.g. see Colesanti et al. (2003a), which provide a comprehensive error budget analysis of the Permanent Scatterers technique. Another topic that is receiving particular attention is the validation of the A-DInSAR results. In general, the validation of the A-DInSAR products is difficult, especially for the extension of the measured areas: often there are no reference data are available. Another complication comes from the relatively high quality of the A-DInSAR and the consequent difficulty to get suitable reference data of higher quality. In the following we briefly refer to the results of projects where the authors directly take or took part. In Crosetto (2004) is described an experiment over a subsidence of small spatial extent, where the deformation was independently estimated twice, by using two ERS SAR datasets, one ascending and one descending. By comparing the two geocoded results, i.e. by performing a kind of repeatability check, it was found a very good agreement between the two deformation maps. Interesting validation results are described in Duro et al. (2005), where, in particular are validated ERS and Envisat results over the main dike of the port of Barcelona illustrated in Figure 7. Finally, it is worth mentioning an ongoing ESA project, named PSIC4 (PS Interferometry Codes Cross Comparison and Certification for Long term differential interferometry), where a several teams will participate by performing a blind test over a deformation area where a rich reference data set coming from traditional geodetic techniques is available.

Satellite	System frequency [GHz]	Start mission	End mission	Wavelength [cm]	DInSAR works based on these data
SEASAT	1.275	1978	1978	23.5	Gabriel, A.K et al. (1989), Li and Goldstein (1990)
ERS-1	5.300	1991	2000	5.6	Massonnet D. et al. (1993), Goldstein et al. (1993)
ERS-2	5.300	1995	2005	5.6	Ferretti A. et al. (2000), Rosen P. A. et al. (2000)
JERS-1	1.275	1992	1998	23.5	Kimura and Yamaguchi (2000), Fujiwara et al. (1998)
RADARSAT-1	5.300	1995	-	5.6	Wegmüller et al. (2000a), Lu et al. (2003)
ENVISAT	5.331	2002	-	5.6	Wegmüller et al. (2000b), Arnaud et al. (2003), Monti Guarnieri et al. (2003)
RADARSAT-2	5.300	*2006*	-	5.6	-

Table 2: Main SAR missions with interferometric SAR capabilities.

8. CONCLUSIONS

In this paper the state-of-the-art of DInSAR techniques for land deformation monitoring has been analysed, discussing the following important aspects:

- the main differences between the standard DInSAR techniques, which are based on the simplest configuration with a single SAR image pair, and the advanced DInSAR techniques, which exploit large sets of images acquired over the same area,
- the importance of the criteria used to select the pixels suitable to estimate the land deformation,
- the availability of DInSAR software tools, and of DInSAR data coming from spaceborne SAR sensors,
- and finally some aspects related to the quality and validation of the DInSAR results.

Different other important topics are not considered in this paper, e.g. an analysis of the limitation of the techniques, the discussion of key technical aspects, such as the phase unwrapping, and the possible synergy with data coming from other sources, etc. This aspects are treated in detail in more comprehensive DInSAR reviews, see Rosen et al. (2000), Bamler and Hartl (1998), and Hanssen (2001). In the following we concisely address two additional topics. The first one is the multidisciplinary character of a lot of the current research related to the DInSAR techniques. DInSAR can be a valuable deformation data source for a plethora of disciplines of earth sciences and engineering: there is a lot of interest and expectation to fully take advantage of the DInSAR outcomes. Due to the rather complex nature of the DInSAR data, the more advanced applications and the best results are usually achieved through a close cooperation between the DInSAR specialists and the people able to interpret, analyse and model the DInSAR. In this context the SAR specialists can play a fundamental role in helping the users of the DInSAR products to fully understand their limits and potentialities. For instance, to understand the huge difference that there is between the qualitative results of a standard DInSAR analysis and those coming from an A-DInSAR procedure. Without this multidisciplinary cooperation there is a risk of treating the DInSAR products as error free (deterministic approach), with the risk of driving wrong conclusions from the rather complex and intrinsically uncertain analyses that are performed in several fields of earth sciences. In the forthcoming years the DInSAR data quality and the uncertainty and sensitivity analyses of the models adopted in the subsequent analyses, e.g. geophysical models, will certainly represent key research issues. A multidisciplinary effort is also required to promote DInSAR as an operational tool for deformation measurements: even if the technique has proved its effectiveness in several application fields, a lot of work is required to promote this new tool and to improve its acceptability by the potential users. An interesting example of cooperation between DInSAR specialists and different geological and geophysical national agencies is given by the project Terrafirma, one of ten services being supported by the European Space Agency's Global Monitoring for Environment and Security (GMES) Service Element Programme, which aims to provide a European ground motion hazard information service, see the project web page: www.terrafirma.eu.com. In this project three types of DInSAR products are proposed: the simple estimation of deformation, a causal interpretation of the deformation phenomenon at hand, and a more advanced modelling stage.

Another interesting issue is given by the different methods and techniques that can complement or improve the results of the spaceborne DInSAR techniques.

- In order to guarantee the DInSAR monitoring of features of special interest, even where there is usually no coherence in the SAR images, it is possible to deploy artificial corner reflectors or active transponders, see Allievi et al. (2004). By installing in situ such devices it is possible to monitor special building, infrastructures, and different types of deformation phenomena that occur in non coherent area (e.g. landslides).
- The use of airborne SAR sensors for differential interferometry is gaining an increasing interest, see e.g. Reigber and Scheiber, (2003). By exploiting longer

wavelengths with better coherence behaviour, like L- or P-band, there is the possibility of analysing long-term processes even in case of vegetated areas. In addition, they offer monitoring capabilities of short-term processes by taking advantage of the typical operational flexibility of airborne sensors. The combination of periodically acquired spaceborne DInSAR images with flexibly acquired airborne data seems to be promising.

- Ground-based SAR interferometry represents an interesting complementary technique. In the last few years terrestrial SAR interferometry based on portable instrumentation has been implemented and validated as a tool for monitoring buildings and structures (Pieraccini et al., 2000; Tarchi et al., 2000), and landslides (Tarchi et al., 2003; Leva et al., 2003). Interesting synergies can be foreseen between ground-based SAR interferometers and airborne and spaceborne SAR systems.

ACKNOWLEDGEMENTS

This work has been partially supported by the Spanish Ministry of Science and Technology, through the research project REN2003-00742, AURORAE. The authors acknowledge Alain Arnaud and Javier Duro from Altamira Information for providing their A-DInSAR results over the city of Barcelona, Riccardo Lanari from IRECE-CNR, Naples, for providing the advanced geocoding results over the San Paolo Stadium of Naples.

REFERENCES

Allievi, J., Prati, C., Rocca, F., Savio, G., Arrigoni, M., Zanoletti, L., 2004. Combined use of artificial and permanent scatterers. *Proceedings of the ESA Envisat Symposium*, 6-10 September 2004, Salzburg (Austria).

Amelung, F., Galloway, D.L., Bell, J.W., Zebker, H.A., Laczniak, R.J., 1999. Sensing the ups and downs of Las Vegas: InSAR reveals structural control of land subsidence and aquifer-system deformation. *Geology*, 27 (6), pp. 483-486.

Amelung, F., Jonson, S., Zebker, H.A., Segall, P., 2000. Widespread uplift and 'trapdoor' faulting on Galápagos volcanoes observed with radar interferometry. *Nature*, 407, pp. 993-996.

Arnaud, A., Adam, N., Hanssen, R., Inglada, J., Duro, J., Closa, J., and Eineder, M., 2003. ASAR ERS interferometric phase continuity. *International Geoscience and Remote Sensing Symposium,* 21-25 July 2003, Toulouse (France), (CDROM).

Bamler, R., Hartl, P., 1998. Synthetic aperture radar interferometry. *Inverse Problems*, 14, R1-R54.

Berardino, P., Fornaro, G., Lanari, R., Sansosti, E., 2002. A new algorithm for surface deformation monitoring based on small baseline differential SAR interferograms*. IEEE Transactions on Geoscience and Remote Sensing,* 40 (11), pp. 2375-2383.

Biescas, E., Agudo, M., Monserrat, O., Ibañez, C., Crosetto, M., 2005. Aplicaciones de la interferometría SAR para la medida de deformaciones del terreno. *Proc. of the 6th. Geomatic Week Conference*, February 2005, Barcelona (Spain), (CDROM, in Spanish).

Carnec, C., Massonnet, D., and King, C., 1996. Two examples of the use of SAR interferometry on displacement-fields of small spatial extent. *Geophys. Res. Lett.*, 23 (24), pp. 3579–3582.

Chorowicz, J., Luxey, P., Rudant, J. P., Lyberis, N., Yürür, T., Gündogdu, N., 1995. Slip-motion estimation along the Ovacik Fault near Erzincan (Turkey) using ERS-1 radar image: evidence of important deformation inside the Turkish plate. *Remote Sensing of Environment*, 52, pp. 66-70.

Colesanti, C., Ferretti, A., Novali, F., Prati, C., Rocca, F., 2003a. SAR monitoring of progressive and seasonal ground deformation using the Permanent Scatterers Technique. *IEEE Transactions on Geoscience and Remote Sensing*, 41 (7), pp. 1685-1701.

Colesanti, C., Ferretti, A., Prati, C., Rocca, F., 2003b. Monitoring landslides and tectonic motions with the Permanent Scatterers Technique. *Engineering Geology*, 68, pp. 3-14.

Crosetto, M., Castillo, M., Arbiol, R., 2003. Urban subsidence monitoring using radar interferometry: Algorithms and validation. *Photogrammetric Engineering and Remote Sensing*, 69 (7), pp. 775–783.

Crosetto M., 2004. Deformation measurement using interferometric SAR data. *Proceedings of the XXth ISPRS Conference*, July 2004, Istanbul (Turkey).

Crosetto, M., Crippa, B., Biescas, E., 2005. Early detection and in-depth analysis of deformation phenomena by radar interferometry. *Engineering Geology* (in press).

Delacourt, C., Allemand P., Squarzoni, C., Picard, F., Raucoules, D., Carnec, C., 2004. Potential and limitation of ERS-Differential SAR Interferometry for landslide studies in the French Alps and Pyrenees. *Proceedings of Fringe 2003 Workshop*, SP-550, ESA (CD-ROM).

Duro, J., Closa, J., Biescas, E., Crosetto, M., Arnaud, A., 2005. High Resolution Differential Interferometry using time series of ERS and ENVISAT SAR data. *Proc. of the 6th. Geomatic Week Conference*, February 2005, Barcelona, Spain (CDROM).

Ferretti, A., Prati, C., Rocca, F., 2000. Nonlinear subsidence rate estimation using permanent scatterers in differential SAR interferometry. *IEEE Transactions on Geoscience and Remote Sensing*, 38 (5), pp. 2202-2212.

Ferretti, A., Prati, C., Rocca, F., 2001. Permanent scatterers in SAR interferometry. *IEEE Transactions on Geoscience and Remote Sensing*, 39 (1), pp. 8-20.

Fruneau, B., Achache, J., Delacourt, C., 1996. Observation and modelling of the Saint-Etienne de Tinee landslide using SAR interferometry. *Tectonophys*, 265 (3–4), pp. 181–190.

Fujiwara, S., Rosen, P., Tobita, M., Murakami, M., 1998. Crustal deformation measurements using repeat-pass JERS-1 synthetic aperture radar interferometry near Izu Peninsula, Japan. *J. Geophys. Res.*, 103, pp. 2411-2424.

Gabriel, A.K., Goldstein, R.M., Zebker, H.A., 1989. Mapping small elevation changes over large areas: differential radar interferometry. *J. Geophys. Res.*, 94 (B7), pp. 9183-9191.

Galloway, D.L., Hudnut, K.W., Ingebritsen, S.E., Phillips, S.P., Peltzer, G., Rogez, F., Rosen, P.A., 1998. Detection of aquifer system compaction and land subsidence using interferometric

synthetic aperture radar, Antelope Valley, Mojave Desert, California. *Water Resources Research*, 34 (10), pp. 2573-2585.

Gatelli, F., Monti Guarnieri, A., Parizzi, F., Pasquali, P., Prati, C., Rocca, F., 1994. The Wavenumber Shift in SAR Interferometry. *IEEE Transactions on Geoscience and Remote Sensing*, 32 (4), pp. 855-865.

Goldstein, R.M., Englehardt, H., Kamb, B., Frolich, R.M., 1993. Satellite radar interferometry for monitoring ice sheet motion: application to an Antarctic ice stream. *Science*, 262, pp. 1525-1530.

Hanssen, R., 2001. *Radar interferometry*. Kluwer Academic Publishers, Dordrecht (The Netherlands).

Hilley, G.E., Bürgmann, R., Ferretti, A., Novali, F., Rocca, F., 2004. Dynamics of Slow-Moving Landslides from Permanent Scatterer Analysis. *Science*, 304, pp. 1952-1955.

Hoffmann, J., Zebker, H.A., Galloway, D.L., Amelung, F., 2001. Seasonal subsidence and rebound in Las Vegas Valley, Nevada, observed by synthetic aperture radar interferometry. *Water Resources Research*, 37 (6), pp. 1551-1566.

Jónsson, S., Adam, N., Bjornsson, H., 1998. Effects of subglacial geothermal activity observed by satellite radar interferometry, *Geophys. Res. Lett.*, 25 (7), pp. 1059–1062.

Jónsson, S., Segall, P., Pedersen, R., Björnsson, G., 2003. Post-earthquake ground movements correlated to pore-pressure transients. *Nature*, 424, pp. 179-183.

Joughin, I.R., Winebrenner, D.P., Fahnestock, M.A., 1995. Observations of ice-sheet motion in Greenland using satellite radar interferometry. *Geophys. Res. Lett.*, 22 (5), pp. 571–574.

Joughin, I., Winebrenner, D., Fahnestock, M., Kwok, R., Krabill, W., 1996. Measurement of ice-sheet topography using satellite radar interferometry. *J. Glaciology*, 42 (140).

Joughin, I.R., Kwok, R., Fahnestock, M.A., 1998. Interferometric estimation of three-dimensional ice-flow using ascending and descending passes. *IEEE Transactions on Geoscience and Remote Sensing*, 36 (1), pp. 25-37.

Joughin, I., Fahnestock, M., Kwok, R., Gogineni, P., Allen, C., 1999. Iceflow of Humboldt, Petermann, and Ryder Gletscher, northern Greenland. *J. Glaciology*, vol. 45, no. 150, pp. 231–241.

Kampes, B. M., Hanssen, R. F., Perski, Z., 2003. Radar Interferometry with public Domain Tools. *Proceedings of Fringe 2003 Workshop*, SP-550, ESA (CD-ROM).

Kimura, H., Yamaguchi, Y., 2000. Detection of landslide areas using satellite radar interferometry, *Photogrammetric Engineering and Remote Sensing*, 66 (3), pp. 337-344.

Kwok, R., Fahnestock, M.A., 1996. Ice sheet motion and topography from radar interferometry. *IEEE Transactions on Geoscience and Remote Sensing*, 34 (1), pp. 189-200.

Lanari, R., Mora, O., Manunta, M., Mallorquí, J.J., Berardino, P., Sansosti, E., 2004. A small-baseline approach for investigating deformations on full-resolution differential SAR interferograms. *IEEE Transactions on Geosciences and Remote Sensing*, 42 (7), pp. 1377-1386.

Le Mouélic, S., Raucoules, D., Carnec, C., King, C., 2005. A least squares adjustment of multi-temporal InSAR data: application to the ground deformation of Paris. *Photogrammetric Engineering and Remote Sensing*, 71 (2), pp. 197-204.

Leva, D., Nico, G., Tarchi, D., Fortuny-Guasch, J., Sieber, A. J., 2003. Temporal analysis of a landslide by means of a ground-based SAR interferometer. *IEEE Transactions on Geoscience and Remote Sensing*, 41, pp. 745 –752.

Li, F. Goldstein, R.M., 1990. Studies of multi-baseline spaceborne interferometric synthetic aperture radars, *IEEE Transactions on Geoscience and Remote Sensing*, 28 (1), pp. 88-97

Lu, Z., Mann, D., Freymueller, J.T., Meyer, D.J., 2000. Synthetic aperture radar interferometry of Okmok volcano, Alaska: Radar observations. *Journal of Geophysical Research*, 105 (B5), pp. 10791-10806.

Lu, Z., Wright, T., Wicks, C., 2003. Deformation of the 2002 Denali Fault Earthquakes, Mapped by Radarsat-1 Interferometry. *EOS*, 84 (41), pp. 430–431.

Massonnet, D., Rossi, M., Carmona, C., Adragna, F., Peltzer, G., Felgl, K., Rabaute, T., 1993. The displacement field of the Landers earthquake mapped by radar interferometry. *Nature*, 364, pp. 138-142.

Massonnet, D., Briole, P., Arnaud, A., 1995. Deflation of Mount Etna monitored by spaceborne radar interferometry. *Nature*, 375, pp. 567-570.

Massonnet, D., Thatcher, W., Vadon, H, 1996. Detection of postseismic fault zone collapse following the Landers earthquake. *Nature*, 382, pp. 489-497.

Massonnet, D., Holzer, T., Vadon, H., 1997. Land subsidence caused by the East Mesa geothermal field, California, observed using SAR interferometry. *Geophys. Res. Lett.*, 24 (8), pp. 901–904.

Massonnet, D., Feigl, K.L., 1998. Radar interferometry and its application to changes in the earth's surface. *Reviews of Geophysics*, 36 (4), pp. 441-500.

Massonnet, D., Sigmundsson, F., 2000. Remote sensing of volcano deformation by radar interferometry from various satellites. In: Mouginis-Mark et al. (eds), Remote sensing of active volcanism. *Geophysical Monographs* 116, American Geophysical Union, pp. 207-221.

Mohr, J.J., Reeh, N., Madsen, S.N., 1998. Three-dimensional glacial flow and surface elevation measured with radar interf. Erometry. *Nature*, 391 (6664), pp. 273–276.

Monti Guarnieri, A., Daria, D., Cafforio, C., Guccione, P., Paquali, P., Nüesch, D., Small, D., Meier, E., Desnos, Y.L. ENVISAT Interferometry for mapping and monitoring: preliminary results. *Proceedings of Fringe 2003 Workshop*, SP-550, ESA (CD-ROM).

Mora, O., Mallorquí, J.J., Broquetas, A., 2003. Linear and nonlinear terrain deformation maps from a reduced set of interferometric SAR images. *IEEE Transactions on Geosciences and Remote Sensing*, 41 (10), pp. 2243 –2253.

Pedersen, R., Sigmundsson, F., Feigl, K.L., Árnadóttir, T., 2001. Coseismic interferograms of two Ms=6.6 earthquakes in the South Iceland Seismic Zone, June 2000. *Geophysical Research Letters*, 28 (17), pp. 3341-3344.

Peltzer, G., Rosen, P., 1995. Surface displacement of the 17 May 1993 Eureka Valley, California earthquake observed by SAR interferometry. *Science*, 268, pp. 1333-1336.

Peltzer, G., Rosen, P., Rogez, F., Hudnut, K, 1996. Postseismic rebound in fault step-overs caused by pore fluid flow. *Science,* 273, pp. 1202-1204.

Peltzer, G., Crampé, F., King, G., 1999. Evidence of the nonlinear elasticity of the crust from Mw7.6 Manyi (Tibet) earthquake. *Science*, 286 (5438), pp. 272-276.

Pieraccini, M., Tarchi, D., Rudolf, H., Leva, D., Luzi, G., Atzeni, C., 2000. Interferometric radar for remote monitoring building deformations. *Electron. Lett*., 36 (6), pp. 569–570.

Reigber, A., Scheiber, R., 2003. Airborne Differential SAR Interferometry: First Results at L-Band. *IEEE Transactions on Geoscience and Remote Sensing*, 41 (6), pp. 1516-1520.

Reilinger, R.E., Ergintav, S., Bürgmann, S., McClusky, S., Lenk, O., Barka, A., Gurkan, O., Hearn, L., Feigl, K.L., Cakmak, R., Aktug, B., Ozener, H., Töksoz, M.N., 2000. Coseismic and postseismic fault slip for the 17 August 1999, M=7.5, Izmit, Turkey earthquake. *Science*, 289 (5484), pp. 1519-1524.

Rignot, E.J., Gogineni, S.P., Krabill, W.B., Ekholm, S., 1997. North and northeast Greenland ice discharges from satellite radar interferometry. *Science*, 276, pp. 934-937.

Rosen, P., Werner, C., Fielding, E., Hensley, S., Buckley, S., Vincent, P., 1998. Aseismic creep along the San Andreas fault northwest of Parkfield, CA measured by radar interferometry. *Geophysical Research Letters*, 25 (6), pp. 825-828.

Rosen, P.A., Hensley, S., Joughin, I.R., Li, F.K., Madsen, S.N., Rodríguez, E., Goldstein, R.M., 2000. Synthetic Aperture Radar Interferometry. *Proceedings of the IEEE*, 88 (3), pp. 333-382.

Salvi, S., Atzori, S., Tolomei, C., Allievi, J., Ferretti, A., Rocca, F., Prati, C., Stramondo, S., Feuillet, N., 2004. Inflation rate of the Colli Albani volcanic complex retrieved by the permanent scatterers SAR interferometry technique. *Geophysical Research Letters*, 31 (12), L12606.

Schröder, R., Puls, J., Hajnsek, I., Jochim, F., Neff, T., Kono, J., Paradella, W.R., Quintino, M., Morisson, D., Pereira, M., 2005. MAPSAR: a small L-band SAR mission for land observation. *Acta Astronautica*, 56 (1-2), pp. 35-43.

Tarchi, D., Rudolf, H., Pieraccini, M., Atzeni, C., 2000. Remote monitoring of buildings using a ground-based SAR: Application to cultural heritage survey. *Int. J. Remote Sens.*, 21 (18), pp. 3545 –3551, 2000.

Tarchi, D., Casagli, N., Fanti, R., Leva, D., Luzi, G., Pasuto, A., Pieraccini, M., Silvano, S., 2003. Landslide monitoring by using ground-based SAR interferometry: An example of application to the Tessina landslide in Italy. *Engineering Geology*, 68 (1-2), pp. 15-30.

Wegmuller U., Strozzi, T. Tosi, L., 2000a. Differential SAR interferometry for land subsidence monitoring: methodology and examples. *Proc. SISOLS 2000,* 25 -29 September 2000, Ravenna (Italy).

Wegmüller U., Strozzi, T. Tosi, L. , 2000b. ERS and ENVISAT differential SAR interferometry for subsidence monitoring. *Proceedings of ERS-ENVISAT Symposium*, 16-20 October 2000, Gothenburg (Sweden).

Wicks, C., Thatcher, W., Monastero, F., Hasting, M., 2001. Steady-state deformation of the Coso Range, East-Central California, inferred from satellite radar interferometry. *Journal of Geophysical Research*, 106 (B7), pp. 13769-13780.

Wright, T., Parsons, B., Fielding, E., 2001. Measurement of interseismic strain accumulation across the North Anatolian Fault by satellite radar interferometry. *Geophysical Research Letters*, 28 (10), pp. 2117-2120.

Zebker, H.A., Rosen, P.A., Goldstein, R.M., Gabriel, A., Werner, C.L., 1994. On the derivation of coseismic displacement fields using differential radar interferometry: The Landers Earthquake. *Journal of Geophysical Research*, 99 (B10), pp. 19617–19634.